HHS Public Access

Author manuscript

Nat Neurosci. Author manuscript; available in PMC 2018 September 19.

Published in final edited form as:

Nat Neurosci. 2018 May ; 21(5): 683–695. doi:10.1038/s41593-018-0120-6.

Lifelong cortical myelin plasticity and age-related degeneration in the live mammalian brain

Robert A. Hill[1,*], **Alice M. Li**[1], and **Jaime Grutzendler**[1,2,*]

[1]Department of Neurology, Yale School of Medicine, New Haven, Connecticut, USA

[2]Department of Neuroscience, Yale School of Medicine, New Haven, Connecticut, USA

Abstract

Axonal myelin increases neural processing speed and efficiency. In adulthood, it is not known if patterns of myelin distribution are fixed or if myelinating oligodendrocytes are continually generated and maintain the capacity for structural remodeling. Using high-resolution intravital label-free and fluorescence optical imaging in the mouse cortex, we demonstrate lifelong oligodendrocyte generation occurring in parallel with structural plasticity of individual myelin internodes. Continuous internode formation occurred on both partially myelinated and unmyelinated axons and the total myelin coverage along individual axons progressed up to two years of age. After peak myelination, gradual oligodendrocyte death and myelin degeneration in aging were associated with pronounced internode loss and myelin debris accumulation within microglia. Thus, cortical myelin remodeling is protracted throughout life, potentially playing critical roles in neuronal network homeostasis. The gradual loss of internodes and myelin degeneration in aging could contribute significantly to brain pathogenesis.

INTRODUCTION

Myelin evolved as a fundamental cellular structure in vertebrate nervous systems that allows saltatory axonal conduction, significantly increasing neural processing speed and energetic efficiency[1,2]. Speed of signal propagation is established by several structural features including axon diameter, myelin thickness, internode length, and node of Ranvier distribution and size[3–5]. Precise developmental modulation of these features allows neural circuits to perform computations such as sound localization in the avian auditory system[6], synchronized electric organ discharge for prey capture by electric fish[7], and isochronicity of signals in mammalian thalamocortical circuits despite variation in projection distances[8]. Therefore, relatively small structural modifications of myelin distribution have the potential to significantly impact neural circuit function. Furthermore, cortical myelination is unique in

*co-corresponding authors: jaime.grutzendler@yale.edu, robert.hill@yale.edu.

AUTHOR CONTRIBUTIONS

R.A.H. and J.G. conceived of and designed all experiments. R.A.H. performed all in vivo imaging and data analysis. A.M.L. performed immunostaining and some fixed tissue imaging. R.A.H. and J.G. wrote the manuscript.

COMPETING INTERESTS

The authors declare no competing financial interests.

its potential to influence synaptic and structural plasticity with proposed roles for myelin related molecules in critical period cessation[9], and heterogeneity in myelin patterning along distinct excitatory[10] and inhibitory[11] neuronal populations.

In addition to being vital for neural circuit formation during developmental stages, oligodendrocytes, the myelinating cells of the central nervous system, maintain a resident progenitor cell population throughout life[12]. These progenitors (NG2-glia), self-renew while continuously generating oligodendrocytes during development and early stages of adulthood[13–18], a process that can be modulated by changes in neural activity and environmental cues[18–22]. It is likely that the production of new oligodendrocytes is involved in sculpting neural circuits, potentially contributing to cellular mechanisms of information storage[23,24]. However, major questions remain about how newly generated cells integrate into an already established adult neural architecture, the extent to which the distribution of myelin internodes in cortical axons is maintained over time, and the degree to which production of new oligodendrocytes persists and myelin plasticity occurs in the adult and aging brain.

We investigated, the lifelong generation of oligodendrocytes and plasticity of myelin segments at individual axonal resolution in the mouse cerebral cortex, using long term intravital myelin imaging with label-free spectral confocal reflectance microscopy (SCoRe)[25] and oligodendrocyte fluorescence reporter transgenic mice. We discovered that oligodendrocyte density continues to increase in the cortex until almost 2 years of age. The generation of new oligodendrocytes results in the continuous filling in of unmyelinated regions in partially myelinated axons. Once formed, the majority of oligodendrocyte internodes are stable over extended intervals. However, a subpopulation of internodes continues to exhibit changes in length over intervals of weeks to months. Imaging in aged mice, revealed a striking decline in myelination, with distinct stages of myelin degeneration including the formation of myelin spheroids, single internode loss, and accumulation of myelin debris within microglia.

Altogether, our data provide direct *in vivo* evidence for long-term structural myelin plasticity with continuous addition of new internodes and structural rearrangement of subpopulations of existing ones throughout life. While the evolutionary purpose and precise function of this protracted process remains unknown, ongoing lifelong myelination could play critical roles in the refinement and plasticity of neuronal networks. In addition, the observed age-related myelin degeneration and axonal internode loss may significantly contribute to cognitive slowing in aging as well as to a variety of neurological disorders. Finally, the methodologies we implemented for tracking oligodendrocytes and internodes for extended intervals in live mice open the possibility of studying myelin plasticity and degeneration with high spatial and temporal precision in a variety of experimental and disease models.

RESULTS

Long-term imaging reveals lifelong addition of oligodendrocytes and myelin internodes

To investigate the long-term plasticity of myelinating oligodendrocytes in the mouse somatosensory cortex, we used a novel strategy combining label-free spectral confocal

reflection (SCoRe) microscopy with concurrent fluorescence imaging of axons and myelinating oligodendrocytes in reporter mice. SCoRe microscopy utilizes the combined signal that arises from the reflection of incident lasers of multiple wavelengths for confocal visualization of compact myelin in a label-free fashion[25,26] (Fig. 1, Supplementary Fig. 1). As previously shown[25], in vivo imaging through a cranial window in mice with fluorescent labeling of a subpopulation of cortical neurons (*Thy1-YFP*) confirmed the specificity of the SCoRe signal for myelinated axons with no reflective signals coming from dendrites or unmyelinated axons (Fig. 1b). Gaps in the SCoRe signal were evident along stretches of single myelinated axons likely corresponding to unmyelinated nodes of Ranvier (Fig. 1c). To further determine the specificity of the SCoRe signal we performed in vivo imaging in mice with membrane tethered EGFP (*Cnp-mEGFP*) or cytoplasmic DsRed (*Plp-DsRed*) labeling of mature oligodendrocytes (Fig. 1d–f, Supplementary Fig. 1). SCoRe signals exclusively co-localized with fluorescently labeled fibers with myelinating internode morphology but not with proximal processes extending from oligodendrocyte cell soma, which are known to be unmyelinated[25] (Fig. 1d–e, Supplementary Fig. 2, Supplementary Video 1). Distinct borders of myelinating processes could be faithfully detected and quantified using SCoRe (Fig. 1f, Supplementary Fig. 2). Comparison of the myelin detection rates using either oligodendrocyte specific mEGFP or SCoRe demonstrated near identical values (Fig. 1g, Supplementary Fig. 2, 159 SCoRe myelin segments, 169 mEGFP myelin segments, 856 SCoRe myelin segment borders, 842 mEGFP myelin segment borders, from n=3 mice). The slightly higher myelin segment density quantified using fluorescence (Fig. 1g) reflects the detection of proximal, non-myelinating, processes with mEGFP labeling in *Cnp-mEGFP* mice (Fig. 1d–e). To further confirm the specificity of the SCoRe signal for myelin, we performed immunohistochemistry on fixed brain tissue sections for contactin associated protein (Caspr), a molecule that localizes to the paranodal regions of oligodendrocyte internodes. As predicted, a break in the SCoRe signal was bordered by bright Caspr-labeled paranodes at nodes of Ranvier and at the edge of the axon initial segment (Fig. 1h–i,). Furthermore, staining with an antibody for myelin basic protein (MBP) showed complete overlap between MBP immunolabeling and SCoRe (Supplementary Fig. 1). Thus, the combination of SCoRe microscopy and fluorescence imaging with genetic labeling of axons and oligodendrocytes provides complementary detailed information about the oligodendrocyte-axon interface in the live mouse brain.

Given the versatility of label-free SCoRe, we first used this technique to quantify how myelination in layer I of the mouse somatosensory cortex changed throughout life. Measurement of the SCoRe signal intensity and length of reflective segments from postnatal day (P)30 to P950 revealed significant changes in myelination, peaking at approximately P640 (Fig. 2, Supplementary Figs. 3–4 n=3–4 mice imaged per age, see Supplementary Table 1 for detailed statistics). Similarly, the density of oligodendrocyte cell bodies visualized in *Plp-DsRed* transgenic mice *in vivo* and by using immunostaining for the oligodendrocyte enzyme 2′,3′-Cyclic-nucleotide 3′-phosphodiesterase (CNPase) in fixed tissues were consistent with the changes observed using SCoRe, with a steady myelination increase peaking at approximately P650 (Fig. 2b–j, Supplementary Figs. 3–4, n=3–4 mice imaged per age, see Supplementary Table 1 for detailed statistics), suggesting that the observed changes in myelin density were due to the addition of new oligodendrocytes rather

than the formation of additional internodes by existing cells. Thus, the accumulation of new oligodendrocytes and myelin internodes is a protracted process that continues until almost two years of age in the mouse cortex.

Plasticity of established myelin internodes

We next investigated the precise patterns of structural plasticity by chronic time-lapse in vivo imaging. We found continuous addition of new myelin internodes resulting from the formation of new oligodendrocytes (Fig. 3a–d), concurrently with some changes in length of single internodes over weeks to months (Fig. 3b–g, Supplementary Fig. 5). Established oligodendrocytes were never observed to sprout entirely new myelinating internodes over 30 days of imaging (n = 166 proximal process from 16 oligodendrocytes from 3 mice, imaged between P70–P100). In contrast, when new internodes formed, this coincided with the emergence of a new adjacent oligodendrocyte (Fig 3c–d). Furthermore, established oligodendrocytes remained extremely stable with no cells disappearing or being replaced over 80 days of time lapse imaging (n = 67 oligodendrocytes from 5 mice imaged between P70–P150). Individual established internodes displayed a variety of behaviors with the majority remaining stable in length for up to 230 days of time-lapse imaging (Fig. 3b), while others extended or retracted over periods of 15–30 days (Fig. 3e). To confirm that the observed changes in internode length were not due to only changes in myelin compaction, as revealed by SCoRe imaging, we repeatedly imaged mature oligodendrocyte processes in *Plp-DsRed* transgenic mice. Consistent with SCoRe imaging, we also observed single internode extension and retraction occurring over days to weeks (Fig. 3f–g). SCoRe imaging of individual myelin internodes between P60 to P90 revealed that 81% were stable, 15% extended, and 4% retracted (Fig. 3h, n=124 myelin segments from 3 mice). During this analysis, we noticed that of the myelin segments that exhibited length plasticity, the vast majority were segments that were adjacent to an unmyelinated portion of the axon, meaning they were not paired with a neighboring internode (Fig. 3i, Supplementary Fig. 2d). After further analysis, we found a clear delineation in the behavior between paired and unpaired segments. Between P60 and P90, 68% of unpaired myelin segments were stable with 25% extending and 7% retracting (Fig. 3i–j). In contrast, 98% of paired myelin segments were stable, with only 2% extending and none retracting (Fig. 3i–j). Thus, the plasticity of myelin internodes is likely restricted by the presence of adjacent stable myelin segments resulting in less plasticity on fully myelinated axons.

To analyze the prevalence of changes in internode length at the single oligodendrocyte level, we performed chronic time-lapse imaging in a transgenic mouse with sparse labeling of mature oligodendrocytes with a membrane tethered GFP (*Plp-creER:mT/mG*) (Fig. 4 and Supplementary Fig. 5), which allows high resolution observation of single myelin internodes in vivo[26] (Fig. 4). To avoid the possibility that the dynamic changes we observed in myelin structure were due to the recent differentiation and immaturity of the oligodendrocyte, we initiated the time lapse imaging 30 days after tamoxifen injections at P30. Thus, all imaged cells had been *Plp*-expressing mature oligodendrocytes for at least 30 days. Consistent with data obtained with SCoRe imaging and in *Plp-DsRed* mice (Fig. 3), we found that the position of oligodendrocyte cell bodies and the majority of myelin internodes were extremely stable, while a small fraction of internodes (~20%) extended or retracted over

days to weeks (Fig 4a–c, Supplementary Fig. 5). We next sought to determine if such changes in internode length were the product of local modulation at the individual internode level or instead reflected a broad expansion of all internodes in their parent oligodendrocyte. We thus tracked multiple internodes in the same individual oligodendrocytes over time and found that they displayed heterogeneous behaviors with some remaining stable, extending, or retracting over a 30-day period (Fig. 4d). Thus, internode plasticity appears to be modulated locally rather than at the entire oligodendrocyte level. Quantification of all cells imaged from P60 to P90 revealed that on average 77±2.4% of all internodes were stable, 17±2.5% extended, and 6±1.3% retracted (n=22 cells, 330 internodes, from 3 mice, mean ± s.e.m) (Fig. 4e). Out of the internodes that did extend or retract, some extended up to 20μm over the 30-day interval (Fig. 4b–f, Supplementary Fig. 5). Thus, using three separate approaches to visualize single oligodendrocyte processes *in vivo* we observed that the vast majority of internodes remain stable with a subpopulation of likely unpaired segments exhibiting some long-term structural plasticity.

Imaging internode distribution along single axons reveals continued addition throughout life

A recent serial electron microscopy reconstruction study of cortical axons in the adult mouse discovered non-uniform distribution of myelin internodes, with significant unmyelinated portions along stretches of individual axons[10]. However, it is not known if such patchy patterns of myelin distribution are maintained over time or if they reflect an intermediate stage in the ongoing adult myelination process. To address this question, we developed a methodology to trace myelin distribution along single axons in the somatosensory cortex up to 1 mm in length, by using a combination of *in vivo* SCoRe imaging and fluorescence imaging of sparsely labeled, layer I axons (Fig. 5a–b, Supplementary Fig. 6). Consistent with the previous study[10], myelinated axons displayed heterogeneous non-uniform myelin coverage at P30–P60, with some axons approaching 80% myelin coverage, while others had only a single myelin segment along the traceable axonal length (Fig. 5c–d, Supplementary Fig. 6). Interestingly, large sections of unmyelinated regions were found on axons at all ages analyzed even up to 640 days old (Fig. 5, Supplementary Fig. 6). On average, however, the myelin coverage along stretches of single axons significantly increased from 43±5% at P30, 49±3% at P60, 62±3% at P220, 68±3% at 370, to 83±2% at P640 (Fig. 5d–e) (P30 n=23 axons, P60 n=72 axons, P220 n=57 axons, P370 n=62 axons, P640 n=62 axons, from 3–4 mice at each age, mean ± s.e.m, see Supplementary Table 1 for detailed statistics).

We next used intravital time-lapse imaging to visualize the longitudinal dynamics of myelin distribution along the same axon. Consistent with the single time point data, we observed filling in of unmyelinated gaps along individual axons slowly proceeding over weeks to months, but we never observed any elimination of existing internodes (Fig. 6). Thus, internode distribution can be modulated throughout life via continual deposition of new myelin segments along single axons due to the generation of new oligodendrocytes. The lack of internode elimination in normal adulthood suggests that myelin plasticity is unlike other forms of structural plasticity in the CNS, such as synaptic remodeling, where both formation and elimination occur concurrently.

Myelin degeneration and internode elimination in advanced aging

Myelin abnormalities occur in normal aging in rodents, monkeys, and humans and may be associated with age-related cognitive decline[27–31]. However, the cellular mechanisms and dynamics of myelin pathology in aging are not well understood and have never been studied at high spatial and temporal resolution in the live mammalian cortex. Using both SCoRe microscopy and fluorescence imaging of mature oligodendrocytes in transgenic reporter mice, we observed a pronounced decrease in oligodendrocyte and myelin density in the cerebral cortex of mice past 2 years of age (Fig 2). Further analysis of this process revealed several intriguing features of degenerating myelin that were highlighted with SCoRe imaging.

First, we detected highly reflective bulbous structures along stretches of otherwise normal appearing myelin segments (Fig. 7a–b, Supplementary Fig. 7). These structures were reminiscent of myelin spheroids seen by electron microscopy in aged brain tissue[32] or myelinosomes seen in models of neuroinflammation and in multiple sclerosis postmortem brain[33]. For the purpose of this study we identified these structures as myelin spheroids. *PLP-DsRed* reporter mice revealed that these reflective spheroid structures co-localized with fluorescent protein accumulations and the oligodendrocyte marker CNPase (Fig 7a–b), suggesting that they had originated from oligodendrocytes rather than axons. Their highly reflective nature suggests that rather than myelin balloons, these spheroids represent focal aberrant accumulations of compact myelin, similar to myelinosomes[33]. Second, we also observed similar reflective structures that were detached from adjacent axons but were co-localized with myelin-derived fluorescent protein in *Plp-DsRed* mice and CNPase antibody staining (Fig 7a–b, Supplementary Fig. 7). Their similarity with spheroids associated with myelinated axons suggests that these structures constituted myelin debris and they could be clearly delineated from oligodendrocyte cell soma based on the lack of nuclear dye labeling (Fig. 7b). Quantification revealed significant age-associated increases in both myelin spheroids and myelin debris (Fig. 7c–d), consistent with the concurrent decline in myelin and oligodendrocyte density (Fig. 2). Finally, using time-lapse imaging in aged mice we observed sequential formation of myelin spheroids, single internode loss, and accumulation of myelin debris (Fig. 7e). Interestingly the formation of myelin spheroids occurred slowly over weeks and once one formed, some remained over at least a month (Fig. 7e), providing further evidence for progressive myelin degeneration over prolonged time frames in the aging cortex. Thus, we describe the distinct phases of protracted myelin degeneration in the aging brain and further establish SCoRe imaging as a powerful tool for label-free in vivo detection of myelin pathology.

Myelin debris accumulation in microglia in advanced aging

Microglia, the resident brain macrophages, are involved in myelin debris removal after injury and in demyelinating diseases such as multiple sclerosis[34]. To investigate how microglia respond to age-related myelin degeneration we performed combined *in vivo* SCoRe and fluorescence imaging in aged dual reporter mice with GFP-labeled microglia and DsRed-labeled oligodendrocytes (*Cx3cr1-GFP:Plp-DsRed*) (Fig. 8, Supplementary Figs. 7–9). Whenever we observed reflective DsRed-labeled myelin debris that were not associated with an established myelin internode, they were almost invariably engulfed by

microglia (60/67 cases from 3 mice) (Fig. 8a–b, Supplementary Figs. 8–9). Microglial engulfment of myelin debris was confirmed by analyzing the microglia-GFP fluorescence surrounding debris in comparison to GFP fluorescence surrounding oligodendrocyte cell bodies as control structures, a measure which we termed microglia proximity index (Fig. 8a–c, Supplementary Figs. 8–9, $P < 0.0001$ n = 67 myelin debris structures and 102 oligodendrocyte cell bodies from 3 mice aged P810, unpaired two-tailed student's t-test). Myelin degeneration and accumulation of debris within microglia was not limited to the cerebral cortex as it was also observed in hippocampus and corpus callosum, suggesting a brain wide phenomenon (Supplementary Fig. 9). Even with substantial accumulation of myelin debris within both processes and cell soma, these microglia maintained short-term surveillance behavior as revealed by time-lapse imaging over minutes (Fig 8e. Supplementary Video 2). In contrast to myelin debris however, microglia displayed no polarization towards or engulfment of myelin spheroids located within existing internode segments (Fig. 8b–d, Supplementary Figs. 8–9, $P = 0.2482$ n = 103 myelin spheroids and 136 internodes from 3 mice, unpaired two-tailed student's t-test). Furthermore, short-term *in vivo* time-lapse imaging of microglia surveillance revealed that process movements were not directed towards or associated with myelin spheroids (Fig. 8e. Supplementary Video 2). The limited interaction between microglia processes and myelin spheroids suggests that microglia do not play an active role in removing disrupted myelin from axons but instead likely accumulate myelin debris through a passive phagocytosis process of shed myelin fragments.

DISCUSSION

Emerging evidence suggests that changes in central nervous system myelination are involved in learning and memory processes with broad implications for plasticity within adult neural circuitry[20,24,35,36]. To date, however, direct *in vivo* evidence of myelin plasticity at the cellular level is lacking. Using a combination of label-free and fluorescence live imaging we discovered several fundamental forms of myelin plasticity occurring in layer I of the mouse cerebral cortex throughout life. First, we described lifelong oligodendrocyte and myelin production as verified with three independent approaches: SCoRe label-free myelin imaging, oligodendrocyte specific *Plp-DsRed* transgenic mice, and immunohistochemistry for the oligodendrocyte specific enzyme CNPase. Second, using both label-free myelin imaging and membrane targeted fluorescent protein labeling of isolated oligodendrocytes we discovered that while the vast majority of oligodendrocytes internodes are stable, a subset displays structural plasticity by lengthening or shortening over weeks to months. These changes in existing internodes, while significant, were more modest compared to the generation of new oligodendrocytes and internodes which was robust over extended intervals. Third, by imaging patterns of myelination along stretches of single axons, we found that myelin distribution was not fixed but instead new internodes continued to be added along partially myelinated axons until late stages of adulthood. Finally, we demonstrate that in aging, there is a marked reversal in the plasticity process such that there is almost no formation of new internodes but instead there are distinct stages of myelin degeneration including spheroid formation, single internode loss, and myelin debris accumulation within microglia. Overall these data suggest that myelination undergoes continual forms of plasticity with protracted

oligodendrocyte formation, internode deposition along single axons and long-term adjustment of internode length well into late stages of normal adulthood, a process that comes to a halt in aging and is associated with stereotypical degenerative features.

A particular challenge for analyses of myelination at the cellular level is a lack of determination of whether or not single internodes produce compact myelin. The SCoRe label-free imaging method in combination with the fluorescence labeling of myelinating oligodendrocytes allows precise determination of when and where compact myelin has formed in the live mouse[25,26]. Several lines of evidence strongly suggest that the SCoRe signal arises from multilayered compact myelin: 1) the SCoRe signal only comes from oligodendrocyte processes with internode morphology and not proximal processes extending from the cell body (Fig. 1, Supplementary Figs. 1–2) 2) the SCoRe signal is not found at the paranode (Fig. 1, Supplementary Fig. 2), unlike membrane tethered fluorescent proteins, thus membrane compaction is likely necessary to generate the reflection 3) the SCoRe signal is dramatically absent or reduced in myelin basic protein knockout shiverer mice[25] which lack the ability to make compact myelin. Using both SCoRe and fluorescence approaches, we discovered that not only were there changes in the localization, density, and length of single oligodendrocyte processes over time, but that the localization of myelin compaction corresponded to the fluorescently labeled myelin internodes. Membrane compaction is necessary for myelination to have a significant effect on signal propagation speed and efficiency, thus by using SCoRe imaging, we can extrapolate that the changes in myelin distribution and length of single internodes that we detected are likely to have a functional consequence on axonal conduction. Previous work has shown changes in white matter structure associated with learning a new task in humans[24,35] and other studies have evidence supporting activity-dependent mechanisms modulating the formation of[18,19,21,22] and axonal selection by[37,38] new oligodendrocytes. Whether or not the specific forms of plasticity we observed here are related to changes in neuronal activity remains to be determined.

The protracted nature of oligodendrocyte generation in cortical layer I has not been specifically addressed by previous studies. There is precedent however for an increase in oligodendrocyte density in adulthood in both mouse and primate white and gray matter[14,16,17,21,28,39,40] in addition to indications of a continual increase in myelin density using magnetic resonance imaging techniques in adult humans[41,42]. Coinciding with oligodendrocyte generation and formation of new internodes, we also observed structural plasticity in a subset of existing myelin internodes that were not paired with adjacent myelinating internodes. There is evidence that average internode lengths are different at various ages[17,28] and change over extended time periods during the remyelination process[43]. To our knowledge, however, this is the first direct evidence in the live mammalian brain that mature myelinating oligodendrocyte processes are capable of structural plasticity under physiological situations. These data were obtained from 2–4 month-old animals and the specificity for the plasticity occurring predominantly by unpaired myelin internodes suggests that this behavior likely declines throughout adulthood as the myelin coverage along single axons progresses. It is possible that oligodendrocytes found in different brain regions behave differently due to genetic diversity resulting in differences in oligodendrocyte production and NG2-glia proliferation[44,45], and myelin internode formation and plasticity[46]. Future investigation will reveal if similar degrees of cortical myelin plasticity to the ones we

observed here occur throughout other brain regions or if this process is unique to the superficial cortex.

Little is known about gray matter myelination, particularly in cortical layer I, despite its likely vital role in the maintenance and plasticity of neocortical circuits. Myelinated axons traversing through layer I originate from various brain regions including subcortical areas such as the thalamus and neighboring cortical regions. Consistent with a recent report in P60 mice[10], we observed heterogeneous myelin profiles along stretches of single axons. These myelin profiles were often characterized by large unmyelinated gaps along partially myelinated axons. Importantly, however, we found that these myelin profiles were not fixed over time as previously suggested[10]. Instead, we observed continual changes in the myelin distribution and coverage along single axons extending to late stages of adulthood. Importantly, we intentionally analyzed a defined population of axons in layer I, those labeled in the *Thy1-YFP* mice, and it remains to be determined if this steady progression in total myelin coverage along stretches of single axons is a brain-wide phenomenon or specific to certain axonal subtypes. The evolutionary purpose and functional consequences of the highly protracted cortical axonal myelination process are not known. One possibility is that these changes represent lifelong cortical circuit refinements resulting in adjustments to signaling speed and efficiency in precise axonal tracts. Another possibility is that given that myelin-associated molecules have been shown to be involved in the cessation of critical periods and in limiting synaptic plasticity[9], a precise balance between optimization of axonal conduction speed and metabolic efficiency through myelination with the consequent loss of plasticity is required to maintain brain homeostasis. Finally, it is also possible that the gradual increase in myelination represents an attempt to compensate for age-related myelin dysfunction, degeneration, and/or changes in energy demands of aging axons, a process which eventually fails, resulting in a decline in myelin and oligodendrocyte density.

Further understanding of the functional roles played by these groups of superficial cortical axons is necessary as their localization at the cortical pial surface and proximity to the meningeal layers makes them uniquely susceptible to both trauma and inflammation in numerous neuropathological conditions[47]. Furthermore, superficial cortex has been reported to be one of the earliest sites of demyelination in multiple sclerosis[48]. The age-related myelin degeneration we observed likely contributes significantly to a decline in processing speed and/or cognitive decline in advanced aging[49]. Thus, the links with human disease in combination with our evidence for lifelong cortical myelin plasticity and degeneration in aging compel further study.

Consistent with a recent report[27], we observed age-dependent myelin debris accumulation in microglia. Interestingly, microglia rarely contacted internodal spheroids, a structure that likely reflects early myelin pathology, but instead appeared to actively phagocytose debris that was either shed from existing internodes or resulted from the death of oligodendrocytes. These data suggest the possibility that myelin degeneration is a cell-autonomous process with microglia not playing an active role in inducing it. However, mutations in genes specific to microglia, such as *Trem2* and *Csf1r*, are known to cause diseases with prominent age-related myelin degeneration suggesting a causal connection[50]. Further studies are necessary to better understand the pathogenic interactions between microglia and myelin in

aging and to determine if myelin debris accumulation within microglia results in microglial dysfunction or if microglia dysfunction exacerbates myelin degeneration. The methodologies for longitudinal myelin imaging that we have developed and our findings showing the lifelong plasticity properties and age-related degeneration of myelin *in vivo* form a strong foundation for future studies.

ONLINE METHODS

Animals

All animal procedures were approved by the Institutional Animal Care and Use Committee (IACUC) at Yale University. Both male and female mice aged P30–P1100 as indicated in the text were used in this study. Mice were housed with 2–5 mice per cage in a 12/12 light/dark cycle, no animals were excluded from analysis. To induce cre recombination in creER transgenic mice a single intraperitoneal injection of tamoxifen (1mg) was given to initiate fluorescent reporter expression in a sparse population of cells at P30. The following transgenic lines were used for fluorescence visualization of oligodendrocyte lineage cells, axons, or microglia. *Plp-DsRed*[51], *Plp-creER*[52] (Jax#005975), *Cnp-mEGFP*[53], *Thy1-YFPh*[54] (Jax#003782), *Thy1-EGFPm*[54] (Jax#007788), *Cx3cr1-GFP*[55] (Jax#005582), and mT/mG[56] (Jax#007586). *PLP-creER*, *Thy1-YFP* and mT/mG mice were on a C57Bl6 background all others were on a mixed C57Bl6- FVB background.

Surgical procedures and in vivo imaging

Chronic cranial windows were used for all in vivo imaging experiments[57]. Briefly animals were anesthetized via intraperitoneal injections of ketamine and xylazine and the skin covering the skull was shaved, sterilized, and removed. A 3mm craniotomy was performed and the skull was replaced by a #0 cover glass. A nut was fixed to the skull and embedded in dental cement for repeated animal immobilization and in vivo imaging. For chronic imaging experiments mice were allowed to recover for three weeks before first time point baseline images were acquired. Similar data were obtained using thinned skull preparations.

In vivo imaging was performed on either an upright confocal laser scanning microscope (Leica SP5) with a 20× water immersion objective (Leica 1.0 NA) for spectral confocal reflection (SCoRe) and fluorescence imaging or a two-photon microscope (Prairie Technologies) with a mode locked tunable MaiTai laser (Spectra Physics) with a 20× water immersion objective (Zeiss 1.0 NA). For SCoRe label free imaging the reflective signal from 488nm, 561nm and 633nm wavelength lasers were combined into a single channel in order to visualize the location of compact myelin[25,26]. Fluorescence signals were captured sequentially using the following wavelengths for single photon excitation: 405nm for DAPI, 488nm for GFP, mGFP and YFP and 561nm for DsRed and mTomato. To acquire data for high resolution in vivo tracing of myelin distribution along single axons, tiled sequential SCoRe and fluorescence images were acquired of the top 75μm of cortical tissue and stitched together in order to acquire a ~1×1mm high resolution image of layer I in the somatosensory cortex. In some cases, for optimal imaging and depth penetration two-photon fluorescence imaging was used primarily for imaging of *Plp-creER:mT/mG* mice. The

following wavelengths were used for two-photon excitation: 900nm- GFP, YFP, mGFP, mTomato, 1020nm- DsRed.

Tissue processing and immunohistochemistry

For fixed tissue analysis mice were anesthetized and perfused with 4% paraformaldehyde followed by 24-hour immersion postfix in the same solution. 50–75μm sections were cut on a vibratome and prepared for immunohistochemistry. Sections were stained in primary antibodies for 3 days (see dilutions below) and corresponding species specific secondary antibodies conjugated to Alexa fluor dyes for 1 day at a dilution of 1:500. All sections were incubated in 5% normal goat serum and 0.1% Triton X-100 in phosphate-buffered saline. The following antibodies were used: Caspr (clone K65/25, 1:500 dilution, cat#75–001, NeuroMab), MBP (synthetic peptide corresponding to Mouse Myelin Basic Protein aa 150, 1:1000 dilution, cat#40390, Abcam), CNPase (clone SMI 91, 1:1000 dilution, cat#836404, Biolegend). CNPase antibody staining required antigen retrieval with 50mM sodium citrate buffer (0.05% Tween 20, pH 6.0) at 95 degrees Celsius for 25 minutes. After staining and PBS wash, sections were mounted and imaged on a Leica SP5 confocal microscope. For fixed tissue SCoRe imaging sections were mounted in a solution of 25% mounting medium (cat#S1964, Dako Ultramount) in PBS and imaged immediately in order to avoid disruption of the refractive index change necessary for sufficient and accurate confocal reflection signals arising from compact myelin.

Statistics quantification and reproducibility

Sample sizes for each group are indicated in the figure legends and in Supplementary Table 1. For SCoRe intensity and length analysis and segmentation, Z projections of 30μm depth from the cortical pial surface were analyzed for all mice. Values were determined automatically using a custom macro in Fiji-ImageJ using robust automatic threshold levels of noise=10, lambda=3, min=208 with binarization to determine density with skeletonization to determine length. One-way ANOVA with Tukey's multiple comparison test was used for statistical analysis. For the overlap between fluorescence and SCoRe in *Cnp-mEGFP* mice we performed two separate analyses. First, we determined the ability to detect myelin segments by independently quantifying the number of mEGFP fibers or SCoRe fibers intersecting a line drawn through an image acquired in vivo from 4 images from n=3 mice (see Supplementary Fig. 2). Second, we determined the ability to detect myelin segment borders using mEGFP and SCoRe by independently quantifying the total number of segment edges using either the fluorescence or SCoRe signal from 4 images from n=3 mice (see Supplementary Fig. 2). A break in a SCoRe signal of at least 3μm was considered a segment border. For *Plp-DsRed* oligodendrocyte density analysis the number of DsRed labeled cell soma were quantified from 4 separate images from Z projections of 30μm depth from the cortical pial surface for each mouse and age group captured from the somatosensory cortex. One-way ANOVA with Tukey's multiple comparison test was used for statistical analysis.

CNPase staining length and intensity quantifications were conducted in 4 mice per age and 8 images were analyzed per mouse and all data was obtained from the first 100μm from the pial surface into layer I of the somatosensory cortex. Non-specific antibody labeling form the glial limitans/dura was excluded from analysis. Length analyses were performed on

single Z sections in the middle of the Z stack and values were determined automatically using a custom macro in Fiji-ImageJ using robust automatic threshold levels of noise=10, lambda=3, min=208 for all images. Intensity analyses were determined by measuring the CNPase fluorescence intensity minus background for randomly selected regions of interest within the first 100μm from the pial surface of the brain. For cell density quantification 3 confocal Z stacks were analyzed per mouse per age group. One-way ANOVA with Tukey's multiple comparison test was used for statistical analysis.

Internode remodeling quantifications were carried out using SCoRe in wild type mice (Fig. 3) and mGFP in *Plp-creER:mT/mG* mice (Fig. 4). For SCoRe quantifications, single myelin segments were randomly chosen and their lengths were repeatedly imaged from P60–P90 and measured relative to the closest intersecting adjacent SCoRe labeled myelin segment. Paired segments were defined as those having an adjacent myelin segment <10μm from the fiber edge. Unpaired segments were defined as those not having an adjacent myelin segment within 10μm from the fiber edge. For *Plp-creER:mT/mG* mice single oligodendrocytes were identified and individual internodes were randomly selected and lengths were measured relative to the closest intersecting adjacent internode as indicated in Figure 5. The same internode was repeatedly imaged and measured from P60–P90 at 10 day intervals. Values were represented as a change in length from baseline with baseline being values determined at the first imaging time point.

Tracing and quantification of myelin coverage along single axons was done in *Thy1-YFP* mice. Fiji-ImageJ simple neurite tracer plugin was used to semi-automatically trace single fluorescently labeled axons and their corresponding SCoRe reflective myelin in layer I of the somatosensory cortex. A gap in the reflective signal greater than 1.5μm was used to designate a break in the myelination and classified as a new SCoRe segment. Only axons with at least one segment of SCoRe labeled myelin were analyzed. One-way ANOVA with Tukey's multiple comparison test was used for statistical analysis.

Myelin spheroids and myelin debris accumulation were quantified in aged mice. Myelin spheroids were defined as a bulbous structure with a diameter at least twice the reflective segment diameter but still connected to a SCoRe reflective segment. Myelin debris were characterized as brightly reflective spheroid structures not connected to a normal appearing SCoRe reflective segment. Density of myelin spheroids and myelin debris were quantified from 4 separate images from Z projections of 30μm depth from the cortical pial surface for each mouse and age group captured from the somatosensory cortex.

Analysis of microglia contact was performed in three heterozygous *Cx3cr1-GFP:Plp-DsRed* double transgenic mice aged to P810. Microglia contact was determined by automatically measuring the microglia GFP fluorescence intensity in a 15-micron dimeter ROI centered on an individual myelin spheroid, normal appearing internode, and myelin debris or normal appearing oligodendrocyte soma as defined above in a single optical z plane. This was used as a surrogate and unbiased approach to determine if there was any preferential microglia process or cell body localization to myelin spheroids and debris which we termed microglia proximity index. Fluorescence intensity values were compared using two-tailed unpaired student's t-tests.

All *in vivo* imaging oligodendrocyte and myelin density quantification data were acquired from acute surgical preparations so cranial window surgery would have no effect on baseline density and length quantifications. All data were assumed to have a normal distribution for each statistical test but this was not formally tested. All data are displayed as mean ± s.e.m. unless otherwise indicated. No data were excluded from analysis, no randomization was used to assign experimental subjects and experimenter blinding was not necessary as the analyses were predominantly automated and/or semi-automated. For oligodendrocyte density quantification, the age of the animal was determined after quantification. No statistical methods were used to pre-determine sample sizes but our sample sizes are similar to those reported in previous publications[18,25,58] and consistent with those used in the field. See the Life Sciences Reporting Summary for more information.

DATA AVAILABILITY

All relevant data are available from the authors upon reasonable request.

Supplementary Material

Refer to Web version on PubMed Central for supplementary material.

Acknowledgments

We thank A. Nishiyama (University of Connecticut) and F. Kirchhoff (University of Saarland) for sharing *PLP-DsRed* transgenic mice. This work was supported by the following grants from the National Institutes of Health: R21NS087511, R21NS088411, R01NS0889734 to J.G., T32NS007224, T32GM007205 to A.M.L., and F32NS090820 and K99NS099469 to R.A.H. This work was also supported in part by a research grant from the National Multiple Sclerosis Society (#RR-1602-07686) to J.G. and a New Vision Award through the Donors Cure Foundation to R.A.H.

References

1. Salzer JL, Zalc B. Myelination. Curr Biol. 2016; 26:R971–R975. [PubMed: 27780071]
2. Nave KA. Myelination and support of axonal integrity by glia. Nature. 2010; 468:244–252. [PubMed: 21068833]
3. Waxman SG. Axon-glia interactions: building a smart nerve fiber. Curr Biol. 1997; 7:R406–10. [PubMed: 9210363]
4. Hutchinson NA, Koles ZJ, Smith RS. Conduction velocity in myelinated nerve fibres of Xenopus laevis. J Physiol (Lond). 1970; 208:279–289. [PubMed: 5500723]
5. Hess A, Young JZ. Correlation of internodal length and fibre diameter in the central nervous system. Nature. 1949; 164:490–491. [PubMed: 18140456]
6. Seidl AH, Rubel EW, Harris DM. Mechanisms for adjusting interaural time differences to achieve binaural coincidence detection. J Neurosci. 2010; 30:70–80. [PubMed: 20053889]
7. Bennett MV. Comparative physiology: electric organs. Annu Rev Physiol. 1970; 32:471–528. [PubMed: 4906125]
8. Salami M, Itami C, Tsumoto T, Kimura F. Change of conduction velocity by regional myelination yields constant latency irrespective of distance between thalamus and cortex. Proc Natl Acad Sci U S A. 2003; 100:6174–6179. [PubMed: 12719546]
9. McGee AW, Yang Y, Fischer QS, Daw NW, Strittmatter SM. Experience-driven plasticity of visual cortex limited by myelin and Nogo receptor. Science. 2005; 309:2222–2226. [PubMed: 16195464]
10. Tomassy GS, et al. Distinct profiles of myelin distribution along single axons of pyramidal neurons in the neocortex. Science. 2014; 344:319–324. [PubMed: 24744380]

11. Micheva KD, et al. A large fraction of neocortical myelin ensheathes axons of local inhibitory neurons. elife. 2016; 5
12. Hill RA, Nishiyama A. NG2 cells (polydendrocytes): listeners to the neural network with diverse properties. Glia. 2014; 62:1195–1210. [PubMed: 24753030]
13. Zhu X, Bergles DE, Nishiyama A. NG2 cells generate both oligodendrocytes and gray matter astrocytes. Development. 2008; 135:145–157. [PubMed: 18045844]
14. Dimou L, Simon C, Kirchhoff F, Takebayashi H, Götz M. Progeny of Olig2-expressing progenitors in the gray and white matter of the adult mouse cerebral cortex. J Neurosci. 2008; 28:10434–10442. [PubMed: 18842903]
15. Kang SH, Fukaya M, Yang JK, Rothstein JD, Bergles DE. NG2+ CNS glial progenitors remain committed to the oligodendrocyte lineage in postnatal life and following neurodegeneration. Neuron. 2010; 68:668–681. [PubMed: 21092857]
16. Zhu X, et al. Age-dependent fate and lineage restriction of single NG2 cells. Development. 2011; 138:745–753. [PubMed: 21266410]
17. Young KM, et al. Oligodendrocyte dynamics in the healthy adult CNS: evidence for myelin remodeling. Neuron. 2013; 77:873–885. [PubMed: 23473318]
18. Hill RA, Patel KD, Goncalves CM, Grutzendler J, Nishiyama A. Modulation of oligodendrocyte generation during a critical temporal window after NG2 cell division. Nat Neurosci. 2014; 17:1518–1527. [PubMed: 25262495]
19. Gibson EM, et al. Neuronal activity promotes oligodendrogenesis and adaptive myelination in the mammalian brain. Science. 2014; 344:1252304. [PubMed: 24727982]
20. Liu J, et al. Impaired adult myelination in the prefrontal cortex of socially isolated mice. Nat Neurosci. 2012; 15:1621–1623. [PubMed: 23143512]
21. Simon C, Götz M, Dimou L. Progenitors in the adult cerebral cortex: cell cycle properties and regulation by physiological stimuli and injury. Glia. 2011; 59:869–881. [PubMed: 21446038]
22. Etxeberria A, et al. Dynamic modulation of myelination in response to visual stimuli alters optic nerve conduction velocity. J Neurosci. 2016; 36:6937–6948. [PubMed: 27358452]
23. McKenzie IA, et al. Motor skill learning requires active central myelination. Science. 2014; 346:318–322. [PubMed: 25324381]
24. Zatorre RJ, Fields RD, Johansen-Berg H. Plasticity in gray and white: neuroimaging changes in brain structure during learning. Nat Neurosci. 2012; 15:528–536. [PubMed: 22426254]
25. Schain AJ, Hill RA, Grutzendler J. Label-free in vivo imaging of myelinated axons in health and disease with spectral confocal reflectance microscopy. Nat Med. 2014; 20:443–449. [PubMed: 24681598]
26. Hill RA, Grutzendler J. In vivo imaging of oligodendrocytes with sulforhodamine 101. Nat Methods. 2014; 11:1081–1082. [PubMed: 25357236]
27. Safaiyan S, et al. Age-related myelin degradation burdens the clearance function of microglia during aging. Nat Neurosci. 2016; 19:995–998. [PubMed: 27294511]
28. Lasiene J, Matsui A, Sawa Y, Wong F, Horner PJ. Age-related myelin dynamics revealed by increased oligodendrogenesis and short internodes. Aging Cell. 2009; 8:201–213. [PubMed: 19338498]
29. Peters A, Kemper T. A review of the structural alterations in the cerebral hemispheres of the aging rhesus monkey. Neurobiol Aging. 2012; 33:2357–2372. [PubMed: 22192242]
30. Bartzokis G. Age-related myelin breakdown: a developmental model of cognitive decline and Alzheimer's disease. Neurobiol Aging. 2004; 25:5–18. [PubMed: 14675724]
31. Sturrock RR. Age-related changes in the number of myelinated axons and glial cells in the anterior and posterior limbs of the mouse anterior commissure. J Anat. 1987; 150:111–127. [PubMed: 3654327]
32. Peters A, Sethares C. Aging and the myelinated fibers in prefrontal cortex and corpus callosum of the monkey. J Comp Neurol. 2002; 442:277–291. [PubMed: 11774342]
33. Romanelli E, et al. Myelinosome formation represents an early stage of oligodendrocyte damage in multiple sclerosis and its animal model. Nat Commun. 2016; 7:13275. [PubMed: 27848954]

34. Kreutzberg GW. Microglia: a sensor for pathological events in the CNS. Trends Neurosci. 1996; 19:312–318. [PubMed: 8843599]
35. Bengtsson SL, et al. Extensive piano practicing has regionally specific effects on white matter development. Nat Neurosci. 2005; 8:1148–1150. [PubMed: 16116456]
36. Fields RD. A new mechanism of nervous system plasticity: activity-dependent myelination. Nat Rev Neurosci. 2015; 16:756–767. [PubMed: 26585800]
37. Hines JH, Ravanelli AM, Schwindt R, Scott EK, Appel B. Neuronal activity biases axon selection for myelination in vivo. Nat Neurosci. 2015; 18:683–689. [PubMed: 25849987]
38. Mensch S, et al. Synaptic vesicle release regulates myelin sheath number of individual oligodendrocytes in vivo. Nat Neurosci. 2015; 18:628–630. [PubMed: 25849985]
39. Peters A, Verderosa A, Sethares C. The neuroglial population in the primary visual cortex of the aging rhesus monkey. Glia. 2008; 56:1151–1161. [PubMed: 18449941]
40. Huang W, et al. Novel NG2-CreERT2 knock-in mice demonstrate heterogeneous differentiation potential of NG2 glia during development. Glia. 2014; 62:896–913. [PubMed: 24578301]
41. Miller DJ, et al. Prolonged myelination in human neocortical evolution. Proc Natl Acad Sci U S A. 2012; 109:16480–16485. [PubMed: 23012402]
42. Haroutunian V, et al. Myelination, oligodendrocytes, and serious mental illness. Glia. 2014; 62:1856–1877. [PubMed: 25056210]
43. Powers BE, et al. Remyelination reporter reveals prolonged refinement of spontaneously regenerated myelin. Proc Natl Acad Sci U S A. 2013; 110:4075–4080. [PubMed: 23431182]
44. Hill RA, Patel KD, Medved J, Reiss AM, Nishiyama A. NG2 cells in white matter but not gray matter proliferate in response to PDGF. J Neurosci. 2013; 33:14558–14566. [PubMed: 24005306]
45. Viganò F, Möbius W, Götz M, Dimou L. Transplantation reveals regional differences in oligodendrocyte differentiation in the adult brain. Nat Neurosci. 2013; 16:1370–1372. [PubMed: 23995069]
46. Bechler ME, Byrne L, Ffrench-Constant C. CNS myelin sheath lengths are an intrinsic property of oligodendrocytes. Curr Biol. 2015; 25:2411–2416. [PubMed: 26320951]
47. Howell OW, et al. Meningeal inflammation is widespread and linked to cortical pathology in multiple sclerosis. Brain. 2011; 134:2755–2771. [PubMed: 21840891]
48. Lucchinetti CF, et al. Inflammatory cortical demyelination in early multiple sclerosis. N Engl J Med. 2011; 365:2188–2197. [PubMed: 22150037]
49. Bartzokis G, et al. Lifespan trajectory of myelin integrity and maximum motor speed. Neurobiol Aging. 2010; 31:1554–1562. [PubMed: 18926601]
50. Yeh FL, Hansen DV, Sheng M. TREM2, microglia, and neurodegenerative diseases. Trends Mol Med. 2017; 23:512–533. [PubMed: 28442216]
51. Hirrlinger PG, et al. Expression of reef coral fluorescent proteins in the central nervous system of transgenic mice. Mol Cell Neurosci. 2005; 30:291–303. [PubMed: 16169246]
52. Doerflinger NH, Macklin WB, Popko B. Inducible site-specific recombination in myelinating cells. Genesis. 2003; 35:63–72. [PubMed: 12481300]
53. Deng Y, et al. Direct visualization of membrane architecture of myelinating cells in transgenic mice expressing membrane-anchored EGFP. Genesis. 2014; 52:341–349. [PubMed: 24851283]
54. Feng G, et al. Imaging neuronal subsets in transgenic mice expressing multiple spectral variants of GFP. Neuron. 2000; 28:41–51. [PubMed: 11086982]
55. Jung S, et al. Analysis of fractalkine receptor CX(3)CR1 function by targeted deletion and green fluorescent protein reporter gene insertion. Mol Cell Biol. 2000; 20:4106–4114. [PubMed: 10805752]
56. Muzumdar MD, Tasic B, Miyamichi K, Li L, Luo L. A global double-fluorescent Cre reporter mouse. Genesis. 2007; 45:593–605. [PubMed: 17868096]
57. Hill RA, Damisah EC, Chen F, Kwan AC, Grutzendler J. Targeted two-photon chemical apoptotic ablation of defined cell types in vivo. Nat Commun. 2017; 8:15837. [PubMed: 28621306]
58. Hill RA, et al. Regional blood flow in the normal and ischemic brain is controlled by arteriolar smooth muscle cell contractility and not by capillary pericytes. Neuron. 2015; 87:95–110. [PubMed: 26119027]

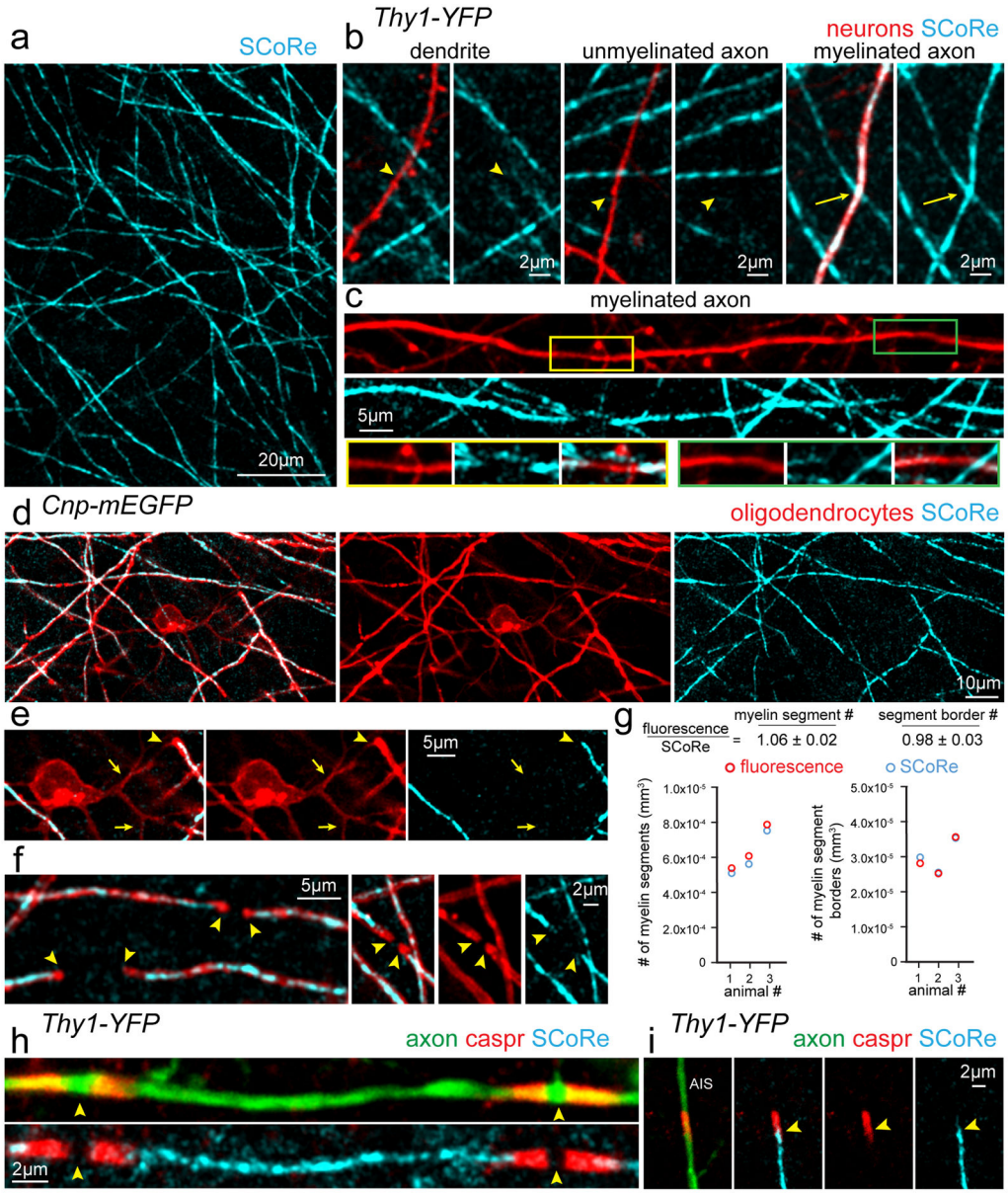

Figure 1. Spectral confocal reflection (SCoRe) microscopy for label-free myelin imaging

(**a**) In vivo image using SCoRe microscopy, captured from layer I of the mouse somatosensory cortex showing single myelin internodes. (**b**) In vivo images captured from a transgenic mouse with sparse YFP fluorescent protein labeling in a subset of neurons (*Thy1-YFP*) showing non-reflective fluorescently labeled dendrites and unmyelinated axons (arrowheads) and a myelinated reflective axon (arrows). (**c**) In vivo image showing unmyelinated gaps (insets) along a regularly myelinated axon further showing the specificity of the SCoRe imaging technique. (**d**) In vivo image captured from a transgenic mouse with membrane tethered EGFP expressed specifically in myelinating oligodendrocytes (*Cnp-mEGFP*) showing complete overlap between fluorescently labeled myelinating internodes and SCoRe. (**e**) In vivo image showing a single oligodendrocyte cell body with proximal, non-myelinating, processes extending from the soma (arrows) and then forming a myelin

sheath revealed by the co-localization of the fluorescent and SCoRe signal (arrowheads). (**f**) The borders of single internodes (arrowheads) are indicated demonstrating the specificity and overlap between oligodendrocyte specific mEGFP and SCoRe. (**g**) Quantification of myelin segments (left) and myelin segment borders (right) detected using either *CNP-mEGFP* fluorescence (red) or SCoRe (cyan) signals demonstrating similar detection of both myelin segments and the borders of single internodes using either the fluorescent label or SCoRe. (159 SCoRe segments, 169 mEGFP segments, 856 SCoRe segment borders, 842 mEGFP segment borders, from n=3 mice) See Supplementary Figure 2 for further example quantification. (**h**) Image of fixed immunolabeled cortical tissue showing a single internode with localization of the paranodal protein Caspr bordering two nodes of Ranvier (arrowheads) and the SCoRe signal arising only from the myelin internode. (**i**) The precise start of SCoRe signal at the edge of the axon initial segment (AIS) adjacent to the Caspr labeling (arrowheads) again showing the precise specificity of the SCoRe signal for myelin. Each image is representative of at least three locations in at least three animals.

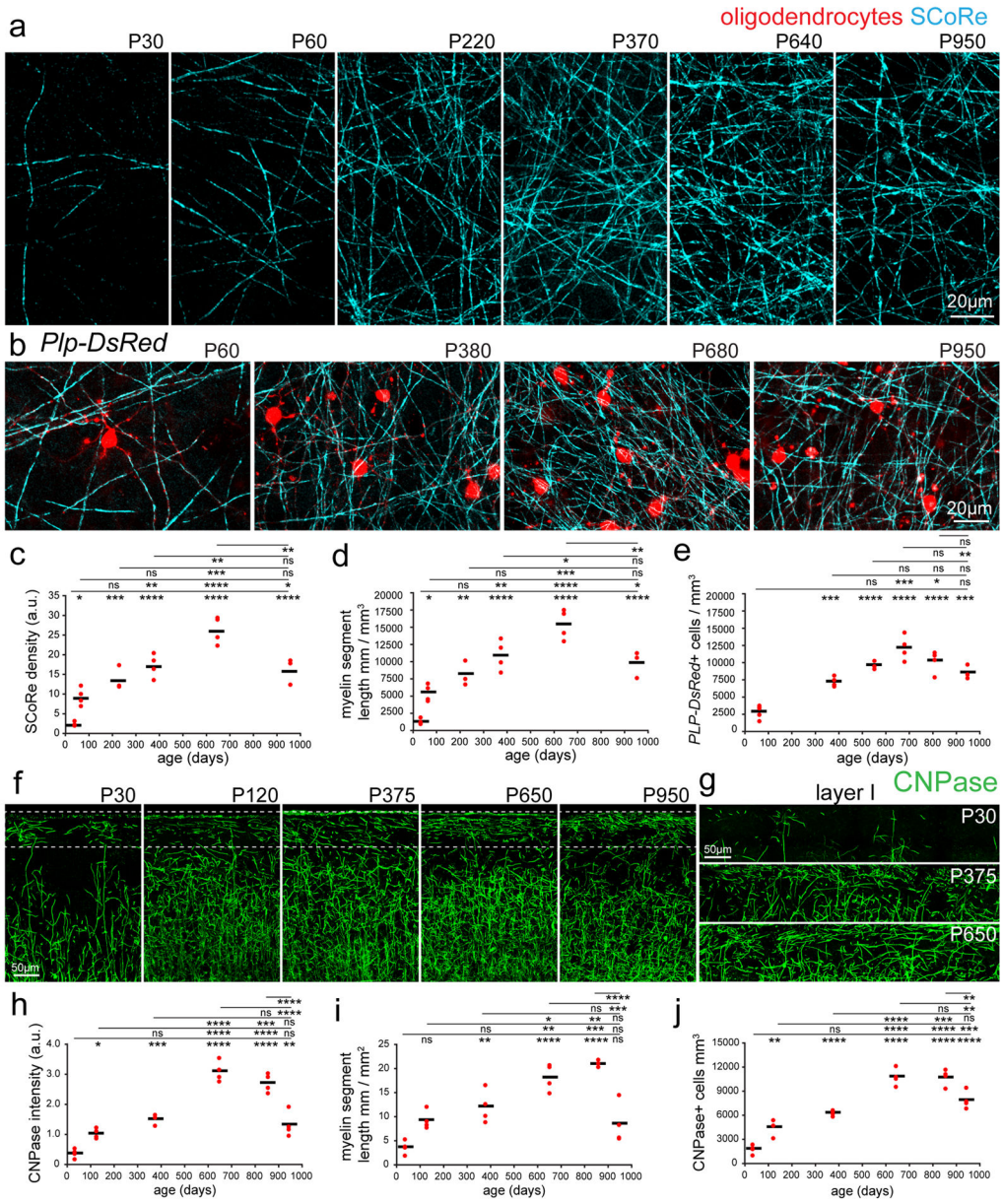

Figure 2. Lifelong changes in cortical myelin and oligodendrocyte density

(**a**) SCoRe images captured *in vivo* at the postnatal day indicated show marked age-dependent changes in myelin density in layer I of the somatosensory cortex. (**b**) In vivo images captured from transgenic mice with DsRed fluorescent protein expressed specifically in mature oligodendrocytes (*Plp-DsRed*), demonstrate age-dependent changes in oligodendrocyte density corresponding to the changes observed in SCoRe signal. (**c**) Average SCoRe reflection density obtained from imaging large regions of interest in vivo at the indicated ages show significant increases in reflective signals until 640 days, followed by a marked decline as the mice age, statistical test: one-way ANOVA with Tukey correction for multiple comparisons. n=3–4 mice per age. (**d**) A measurement of myelination length per volume unit derived from SCoRe images at the indicated ages shows a gradual increase in

the total myelin segment length per area until 640 days, followed by a decline in aging, statistical test: one-way ANOVA with Tukey correction for multiple comparisons, n=3–4 mice per age. (**e**) Oligodendrocyte imaging (*Plp-DsRed*+ cells) at the indicated ages show significant increases in oligodendrocyte density until 640 days followed by a decrease as the mice age, statistical test: one-way ANOVA with Tukey correction for multiple comparisons, n=3–6 mice per age. (**f–g**) Images of oligodendrocyte specific CNPase staining captured from the somatosensory cortex showing age-dependent changes in layer I of the cortex (boxed regions). (**h**) CNPase staining density at the indicated ages showing significant increases in fluorescence signal until P650, followed by a marked decline in aging, statistical test: one-way ANOVA with Tukey correction for multiple comparisons. n=4 mice per age, each red dot indicates one mouse. (**i**) CNPase process length per volume at the indicated ages showing significant increases in the total myelin segment length until 650 days, statistical test: one-way ANOVA with Tukey correction for multiple comparisons, n=4 mice per age. (**j**) CNPase+ oligodendrocyte density at the indicated ages showing significant increases in oligodendrocyte density until 650 days, with a significant decline in aging, statistical test: one-way ANOVA with Tukey correction for multiple comparisons, n=4 mice per age, in all graphs each red dot indicates one mouse and the horizontal line indicates the mean. NS = not significant, * = P<0.05, ** = P<0.01, ***P<0.001, ****P<0.0001, lines indicate mean. Descriptive statistics can be found in Supplementary Table 1. Each image is representative of at least three locations in at least three animals.

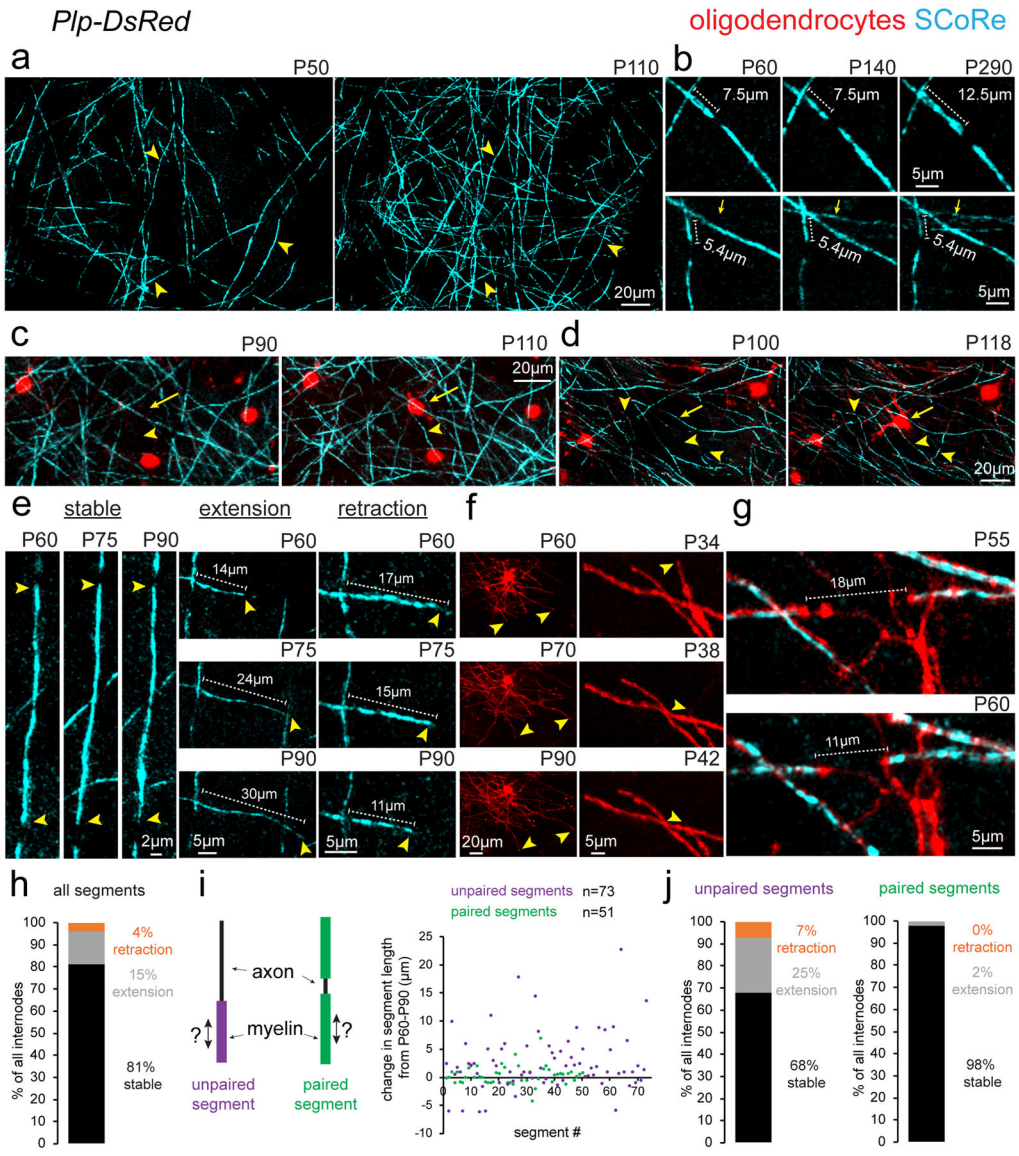

Figure 3. Protracted addition of new internodes and long-term myelin sheath plasticity

(**a**) Time lapse in vivo SCoRe microscopy at the postnatal day indicated shows the appearance of numerous newly reflective internodes. Arrowheads indicate the location of the same axons at different time points. (**b**) Repeated in vivo imaging of changes in compact myelin over 230 days showing the addition of new myelinating internodes (arrows) and the stability or plasticity of presumptive nodes of Ranvier as myelin internode length changes. (**c–d**) Longitudinal time-lapse *in vivo* imaging shows the emergence of new oligodendrocytes (arrows) correlating with the formation of new SCoRe-positive internodes (arrowheads). (**e**) Time-lapse images showing the three types of observed behaviors for internode length dynamics (stable, extension, or retraction). Arrowheads indicate the ends of myelin segments with lengths of single segments indicated (dotted lines). (**f**) In vivo time-lapse images of oligodendrocytes in *Plp-DsRed* mice showing changes in internode length (arrowheads) at the postnatal age indicated. (**g**) In vivo time-lapse images of adjacent

internodes (arrowheads) getting closer over time. (**h**) Breakdown of all SCoRe labeled myelin segment plasticity behavior between P60 to P90 (n=124 myelin segments from 3 mice). (**i**) Diagram showing the definition of a paired or unpaired myelin segment and the total change in length of all segments imaged between P60–P90, each dot represents one myelin segment. (**j**) Breakdown of myelin segment plasticity behavior separated into paired or unpaired subgroups demonstrating that the vast majority of segment length change over time occurs by unpaired myelin segments. Each image is representative of at least three locations in at least three animals.

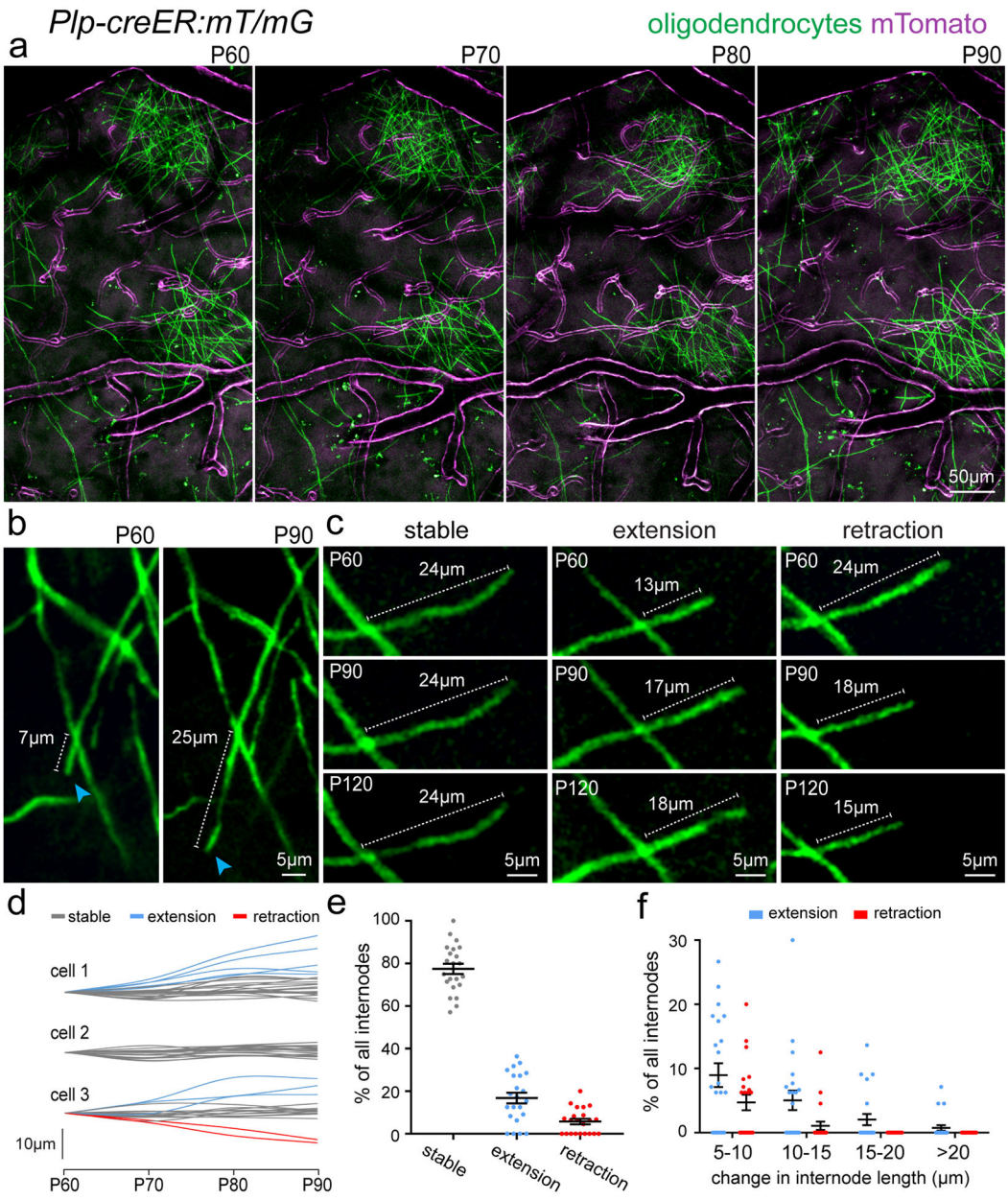

Figure 4. Evidence of myelin plasticity through internode remodeling

(**a**) In vivo two-photon fluorescence images of single oligodendrocytes imaged over 30 days in a transgenic mouse line (*Plp-creER:mT/mG*) with membrane tethered GFP (mGFP) expressed specifically in mature oligodendrocytes and membrane tethered Tomato (mTomato) expressed predominantly in cerebral blood vessels. (**b**) In vivo time-lapse images showing extension of a single internode (blue arrowheads) with stability of all other internodes in the field of view. (**c**) In vivo time-lapse images showing the three observed behaviors for internode length changes over time. (**d**) Measurements of changes in single internode length for individual oligodendrocytes as indicated. Single cells exhibited heterogeneous internode plasticity over the 30 days of imaging with single internodes remaining stable (gray lines), extending (blue lines), or retracting (red lines). (**e–f**)

Distribution of the single internode behavior in all cells. The vast majority of internodes showed no change (>5μm) in length however a proportion displayed long-term extension or retraction over the imaging period ranging from 5–20μm changes over 30 days of imaging as indicated, data represent 22 individual oligodendrocytes, 330 internodes, from 3 mice. Dots indicate single oligodendrocytes and error bars are mean +/− s.e.m., each image is representative of at least three locations in at least three animals.

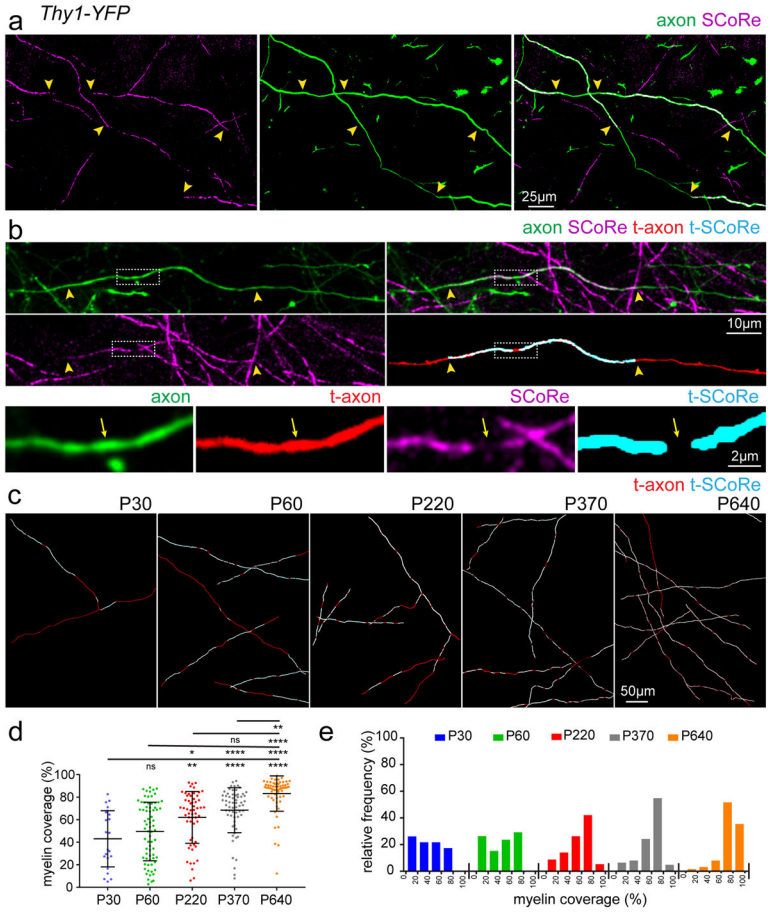

Figure 5. Lifelong changes in myelin coverage along single cortical axons

(**a**) In vivo image captured from the cortex of a P30 *Thy1-YFP* transgenic mouse showing two partially myelinated axons designated by the discontinuous SCoRe signal arising from regions of the axon not covered by a myelin segment (yellow arrowheads). (**b**) In vivo images showing a single axon that was imaged with SCoRe and traced to determine the distribution of myelin along the axon. High magnification insets showing the precise location and distribution of compact myelin (t-SCoRe = traced SCoRe, t-Axon = traced axon) along the single axon. Arrows indicate the end of the myelinating internodes and arrowheads indicate a node of Ranvier. (**c**) Representative traced axons from mice at the ages indicated showing age-dependent increase in myelin coverage along single axons. (**d**) Grouped data showing the percent myelin coverage of single axons imaged at the designated age, statistical test: one-way ANOVA with Tukey correction for multiple comparisons. (**e**) Relative frequencies of single axon myelin coverage at the designated ages showing a protracted shift in total axon coverage with age. Sample size (n) for quantification for (d–e): P30=23 axons from 4 mice, P60=72 axons from 4 mice, P220=57 axons from 3 mice, P370=62 axons from 4 mice, and P640=62 axons from 4 mice. Dots indicate single axons. NS = not significant, * = P<0.05, ** = P<0.01, ***P<0.001, ****P<0.0001 error bars are mean +/− s.e.m., descriptive statistics can be found in Supplementary Table 1. Each image is representative of at least three locations in at least three animals.

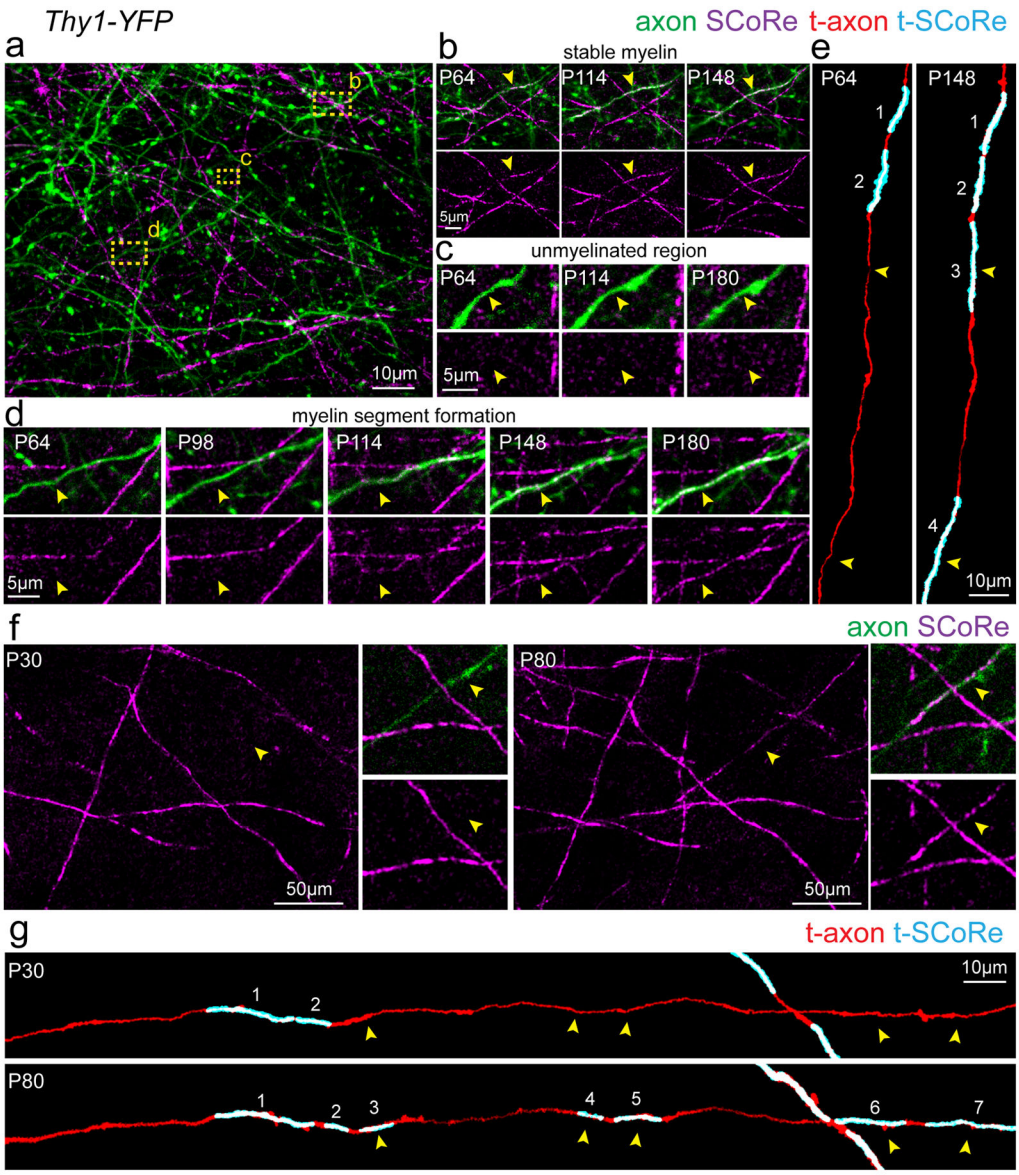

Figure 6. Continuous myelin deposition along partially myelinated axons

(**a**) In vivo SCoRe and fluorescence image captured from the cortex of a P64 *Thy1-YFP* transgenic mouse showing the patchy myelin distribution along a single axon designating the regions highlighted in panels (b–d). (**b**) Repeated imaging of the region designated in panel (a) showing stable myelination (arrowheads) on this portion of the imaged axon over 84 days of imaging. (**c**) Repeated imaging of the region designated in panel (a) showing a region along the same axon that remains unmyelinated (arrowheads) over the 116 days of imaging. (**d**) Repeated imaging of the region designated in panel (a) showing a region along the same axon that becomes myelinated (arrowheads) during the 116 days of imaging. (**e**) Semi-automatic axonal myelin distribution reconstructions of the axon depicted in (a–d) showing the addition of new myelin segments (arrowheads). Numbers indicate the same myelin segment. (**f**) In vivo SCoRe and fluorescence time-lapse images showing the formation of a new myelin segment along a single *Thy1-YFP* fluorescently labeled axon (arrowheads). (**g**)

Semi-automatic axonal myelin distribution reconstruction of the axon designated in (f) showing the formation of several myelin segments along the traced axon (arrowheads) with other regions remaining unmyelinated over the 50 days of imaging. Numbers indicate the same myelin segment. Each image is representative of at least three locations in at least three animals.

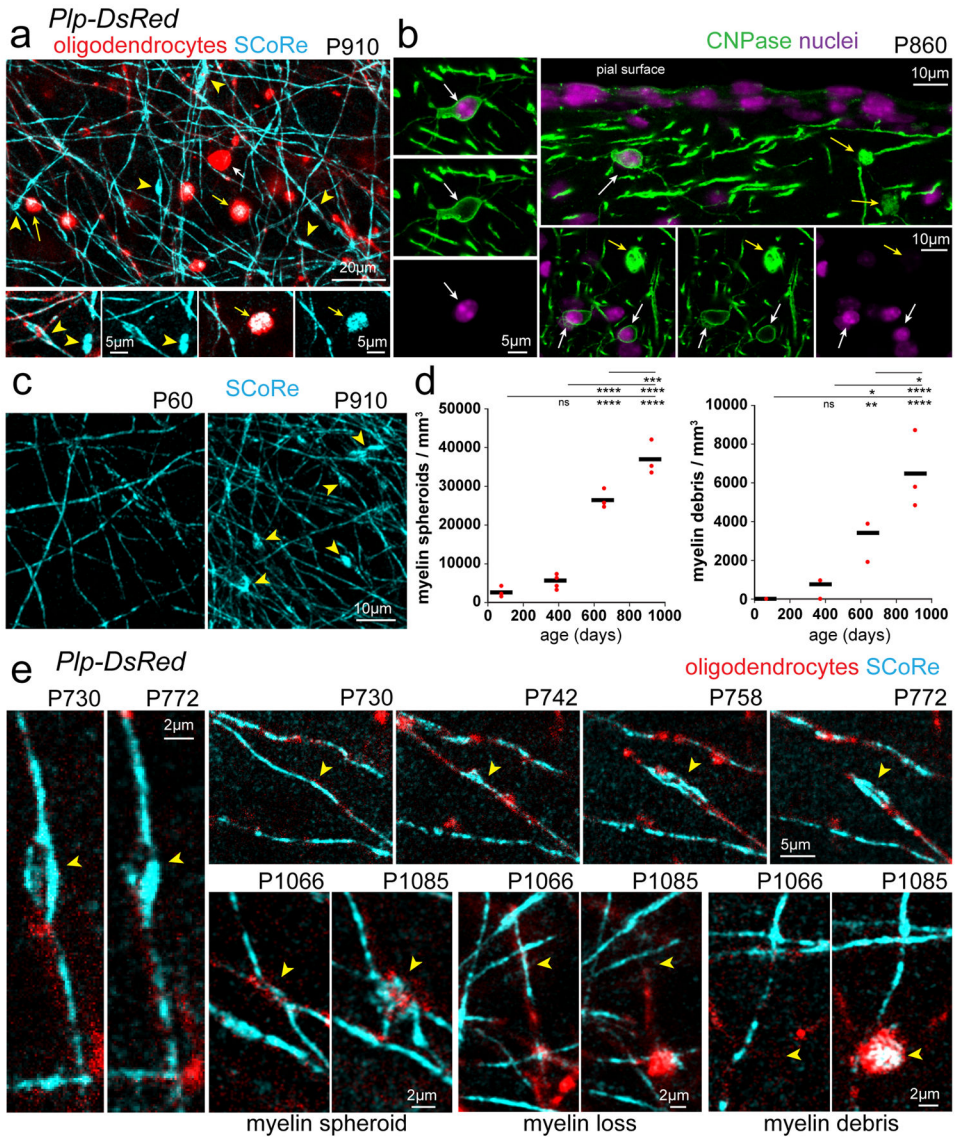

Figure 7. Oligodendrocyte and myelin degeneration in advanced aging

(**a**) In vivo images captured from the cortex of a 910-day old mouse with mature oligodendrocytes labeled with DsRed (*Plp-DsRed*). Examples of myelin pathology detected in aged mice revealed by SCoRe label free imaging and DsRed fluorescence in or derived from oligodendrocytes. Myelin spheroids (yellow arrowheads) can be detected using SCoRe and are only found in aged mice. Myelin debris (yellow arrows) can also be detected using SCoRe and the vast majority were found to have accumulation of DsRed fluorescent protein in the *Plp-DsRed* transgenic mice suggesting a myelin origin. Myelin debris (yellow arrows) and oligodendrocyte cell bodies (white arrows) can be distinguished due to the lack of SCoRe signals in addition to the proximal processes extending from the cell soma. (**b**) Images captured from tissue sections immunostained for oligodendrocyte specific CNPase showing the distinction between myelin debris (yellow arrows) and oligodendrocyte cell bodies (white arrows) confirmed via nuclear dye labeling. (**c–d**) Age-dependent increase in

the presence of myelin spheroids (yellow arrowheads) and myelin accumulations, statistical tests: one-way ANOVA with Tukey correction for multiple comparisons n=3–4 mice per age. NS = not significant, * = P<0.05, ** = P<0.01, ***P<0.001, ****P<0.0001. Each dot indicates one mouse and horizontal lines indicate the mean (**e**) In vivo time lapse images showing the dynamics of age-related myelin pathology (yellow arrowheads) with some myelin spheroids remaining stable, formation of myelin spheroids, single fiber loss, and myelin debris accumulations. Descriptive statistics can be found in Supplementary Table 1. Each image is representative of at least three locations in at least three animals.

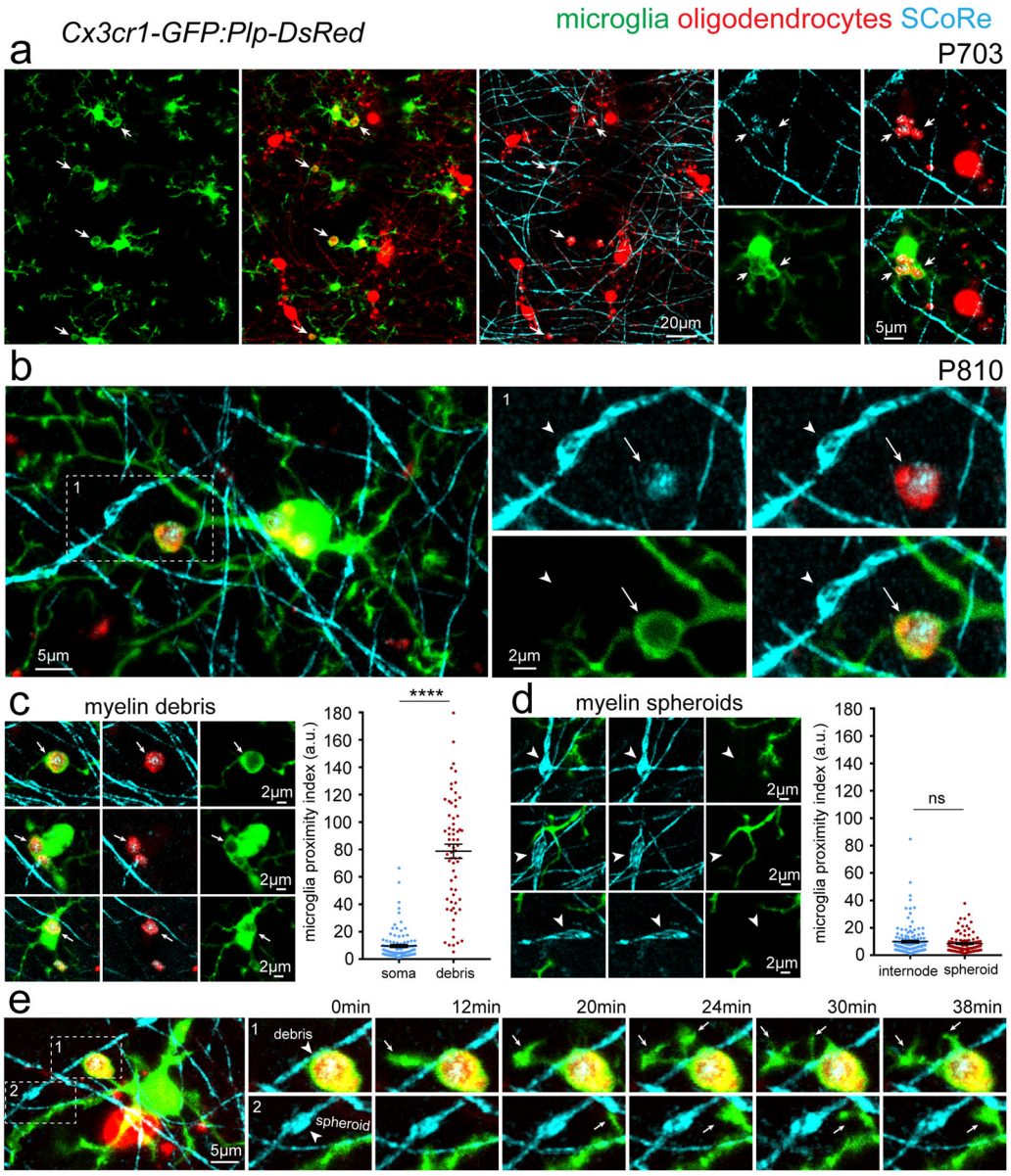

Figure 8. Myelin debris accumulate in microglia in advanced aging

(**a**) In vivo combined SCoRe and fluorescence images from aged (P703) dual reporter transgenic mice with GFP-labeled microglia and DsRed-labeled oligodendrocytes (*Cx3cr1-GFP:Plp-DsRed*) arrows indicate myelin debris accumulations within microglia (**b**) In vivo image showing accumulation of reflective and DsRed labeled myelin debris within a single microglial process (arrow) but not microglial contact to the immediately adjacent myelin spheroid (arrowhead). (**c**) Examples images of myelin debris accumulations in GFP labeled microglia (arrows) and quantification of microglia-GFP fluorescence intensity (microglia proximity index) surrounding myelin debris which was not found around intact oligodendrocyte soma (**** $P < 0.0001$ n = 67 myelin debris structures and 102 oligodendrocyte soma from 3 mice aged P810, unpaired two-tailed student's t-test) each dot indicates one debris or one oligodendrocyte soma and error bars are mean +/− s.e.m. (**d**)

Example images of myelin spheroids (arrowheads) with no microglia process polarization, association, or engulfment with quantification showing no difference in microglia-GFP fluorescence intensity (microglia proximity index) surrounding myelin spheroids or normal appearing myelin internodes (NS = not significant P = 0.2482, n = 103 myelin spheroids and 136 internodes from 3 mice, unpaired two-tailed student's t-test) each dot indicates one spheroid or internode and error bars are mean +/− s.e.m. (**e**) *In vivo* time-lapse images of the boxed regions showing dynamic microglia surveillance with filopodia (arrows) extending from a single process filled with myelin debris (arrowhead in top image sequence) and no directed microglia surveillance of an adjacent myelin spheroid (arrowhead in bottom image sequence). Descriptive statistics can be found in Supplementary Table 1. Each image is representative of at least three locations in at least three animals.